Computer Physics Communications 214 (2017) 225–230

Contents lists available at ScienceDirect

Computer Physics Communications

journal homepage: www.elsevier.com/locate/cpc

Mie calculation of electromagnetic near-field for a multilayered sphere☆

Konstantin Ladutenko [a,b], Umapada Pal [c], Antonio Rivera [d], Ovidio Peña-Rodríguez [c,d,*]

[a] ITMO University, 49 Kronverskii Ave., St. Petersburg 197101, Russian Federation

[b] Ioffe Physical-Technical Institute of the Russian Academy of Sciences, 26 Polytekhnicheskaya Str., St. Petersburg 194021, Russian Federation

[c] Instituto de Física, Universidad Autónoma de Puebla, Apartado Postal J-48, Puebla, Puebla 72570, Mexico

[d] Instituto de Fusión Nuclear, Universidad Politécnica de Madrid, C/ José Gutiérrez Abascal 2, E-28006 Madrid, Spain

ARTICLE INFO

Article history:
Received 17 June 2015
Received in revised form
17 January 2017
Accepted 20 January 2017
Available online 6 February 2017

Keywords:
Mie scattering
Multilayered sphere
Near-field calculation

ABSTRACT

We have developed an algorithm to calculate electric and magnetic fields inside and around a multilayered sphere. The algorithm includes explicit expressions for Mie expansion coefficients inside the sphere and calculation of the vector spherical harmonics in terms of the Riccati–Bessel functions and their logarithmic derivatives. This novel approach has been implemented in the new version of our program *scattnlay*. *Scattnlay* 2.0 will be the first publicly available (at GitHub, https://github.com/ovidiopr/scattnlay) program, based on the Mie theory, which can calculate near-fields for the general case of a multilayer sphere. Several tests were designed to verify that the results obtained with our code match literature results and those obtained through similar programs (limited to core-shell structures) or full-wave 3D simulations. These tests demonstrate that the implementation is effective, yielding accurate values of electric and magnetic fields for a wide range of size parameters, number of layers, and refractive indices.

Program summary

Program title: scattnlay 2.0

Catalogue identifier: AEEY_v2_0

Program summary URL: http://cpc.cs.qub.ac.uk/summaries/AEEY_v2_0.html

Program obtainable from: CPC Program Library, Queen's University, Belfast, N. Ireland

Licensing provisions: GNU GPL v3

No. of lines in distributed program, including test data, etc.: 34502

No. of bytes in distributed program, including test data, etc.: 851543

Distribution format: tar.gz

Programming language: C++11.

Computer: Any computer with a C++11 compiler.

Operating system: Linux (any version), Windows, Solaris.

RAM: 1 Mb–100 Mb

Classification: 1.3.

Does the new version supersede the previous version?: Yes

Nature of problem: The scattering of electromagnetic (EM) radiation by a multilayered sphere is an interesting phenomenon which has recently drawn a great attention for application of tailor-made nanostructures in several fields like medicine (optical imaging and photothermal cancer therapy), atmospheric sciences (to study light absorption by aerosols), design of invisibility cloaks, etc. Expressions of scattering coefficients seem to be simple and straightforward to implement; however, they involve

☆ This paper and its associated computer program are available via the Computer Physics Communication homepage on ScienceDirect (http://www.sciencedirect.com/science/journal/00104655).

* Corresponding author at: Instituto de Fusión Nuclear, Universidad Politécnica de Madrid, C/ José Gutiérrez Abascal 2, E-28006 Madrid, Spain.
E-mail address: ovidio.pena@upm.es (O. Peña-Rodríguez).

http://dx.doi.org/10.1016/j.cpc.2017.01.017

several numerical difficulties that make most of the existent algorithms inapplicable to several common cases. An improved recursive algorithm that circumvents most of the numerical problems present in previous algorithms has been developed by Yang [1]. This algorithm has been implemented in our program [2] to calculate the far-field parameters. In the updated version we have developed and implemented an efficient algorithm for the calculation of electric and magnetic fields inside and around multilayered spheres. In addition to the near-field calculations, the program includes some new functionalities, such as the possibility of including a layer composed of a perfect electrical conductor.

Solution method: Calculation of Mie scattering coefficients and efficiency factors for a multilayered sphere as described by Yang [1], combined with standard solutions of the scattering amplitude functions. Determination of electric and magnetic fields using an algorithm developed in this work.

Reasons for new version: To include calculations of electric and magnetic fields inside and around the particle.

Summary of revisions: The code has been ported to C++11, which has given a cleaner and faster implementation. A new algorithm has been devised and implemented to include the calculation of near electric and magnetic fields. Finally, several small bug fixes and improvements to the original code have been made.

Restrictions: Single scattering and permeability of the layers fixed to unity. Large complex part of layers refractive index leads to convergence problems.

Running time: Seconds to minutes

References:

[1] W. Yang, Appl. Opt. 42 (2003) 1710–1720.
[2] O. Peña, U. Pal, Comput. Phys. Commun. 180 (2009) 2348–2354.

1. Introduction

Scattering of electromagnetic (EM) radiation by a multilayered sphere is a very interesting phenomenon with applications in several areas. In plasmonics, for instance, various types of nanoshells (alternating layers of dielectric and metal) have been extensively studied [1–4] due to their potential for applications in cancer treatment [5,6] and medical diagnostics [7]. In atmospheric science, on the other hand, light absorption by aerosols has a heating effect that is of great interest for studying several climatic effects. These aerosols have been successfully modelled as multilayered spheres, containing water and soot [8,9]. Finally, this model has also been used to design "invisibility cloaks" based on several dielectric layers [10].

Hence, it is not surprising that several algorithms have been developed to solve the problems related to EM scattering by core-shell [11,12] and multilayered [13–20] spheres. Probably for historical reasons most of the existing models focus on far-field (these parameters are easier to measure), somewhat neglecting near-field effects, in spite of their importance in phenomena such as surface enhanced Raman scattering [21], and its potential for a better understanding of several other effects [22,23]. Some algorithms have been devised for near-field calculation in core-shell structures [24,25] but, to the best of our knowledge, there exists no algorithm based on Mie theory for solving the case of EM scattering by multilayered spheres considering both near-field and far-field cases.

In this work, we have developed explicit equations of the expansion coefficients for all the layers of a stratified particle. These coefficients can be used to calculate complex electric and magnetic fields at any point inside and around the particle. All the calculations were implemented in the new version (2.0) of our computer program *scattnlay* [26]. Various tests were performed on the code to ensure its stability and reliability. Finally, we describe several improvements that have been made and added to *scattnlay*, to increase its application areas and/or processing speed.

2. EM fields in a multilayered sphere

Electric and magnetic fields can be calculated for an incident x-polarized plane wave, $\mathbf{E}_i = E_0 \exp[ikr\cos(\theta)]\hat{\mathbf{e}}_x$ with time dependence $\exp(-i\omega t)$ impinging on a multilayered sphere. Each layer of the sphere is characterized by its size parameter $x_l = 2\pi n_m r_l/\lambda = kr_l$ and relative refractive index $m_l = n_l/n_m$, $l = 1, 2, \ldots, L$, where λ is the wavelength of the incident wave in vacuum, r_l is the outer radius of the lth layer, n_m and n_l are the refractive indices of the medium outside the particle and its lth component, respectively, and k is the propagation constant. The relative refractive index m_{L+1} is equal to unity in the region outside the particle. The whole space is divided into two regions: the region inside the multilayered sphere, and the surrounding medium outside the particle. The electric and magnetic fields can be considered as the superposition of inward and outward sets of spherical wave functions. For example, $\mathbf{E}_{in}$ and $\mathbf{E}_{out}$ can be expressed in terms of complex spherical eigenvectors [17,26]:

$$\mathbf{E}_{in} = \sum_{n=1}^{\infty} E_n \left[c_n^{(l)} \mathbf{M}_{o1n}^{(1)} - i\, d_n^{(l)} \mathbf{N}_{e1n}^{(1)} \right] \tag{1.1}$$

$$\mathbf{E}_{out} = \sum_{n=1}^{\infty} E_n \left[i\, a_n^{(l)} \mathbf{N}_{e1n}^{(3)} - b_n^{(l)} \mathbf{M}_{o1n}^{(3)} \right], \tag{1.2}$$

where $E_n = i^n E_0 (2n+1)/(n(n+1))$, and $\mathbf{M}_{o1n}^{(j)}$ and $\mathbf{N}_{e1n}^{(j)}$ $(j = 1, 3)$ are the vector spherical harmonics and superscripts denote the kind of Bessel function (z_n); it can be either (1), for the first kind of spherical Bessel function (j_n), or (3), for the first kind of spherical Hankel function ($h_n^{(1)}$). Likewise, vector spherical harmonics are usually defined in terms of the first kind of spherical Bessel and Hankel functions [12], but their evaluation is very tricky, due to the peculiar behaviour (i.e., convergence problems) of those functions. This is particularly true for complex arguments with a large imaginary part, which often arise in Mie calculations. We have re-stated the vector spherical harmonics in terms of the

Riccati–Bessel functions and their logarithmic derivatives, which are much more tractable:

$$\mathbf{M}_{o1n}^{(j)} = \cos\phi\,\pi_n(\cos\theta)\,\frac{r_n(\rho)}{\rho}\hat{\mathbf{e}}_\theta - \sin\phi\tau_n(\cos\theta)\,\frac{r_n(\rho)}{\rho}\hat{\mathbf{e}}_\phi \tag{2.1}$$

$$\mathbf{M}_{e1n}^{(j)} = -\sin\phi\,\pi_n(\cos\theta)\,\frac{r_n(\rho)}{\rho}\hat{\mathbf{e}}_\theta - \cos\phi\tau_n(\cos\theta)\,\frac{r_n(\rho)}{\rho}\hat{\mathbf{e}}_\phi\,, \tag{2.2}$$

$$\mathbf{N}_{o1n}^{(j)} = \sin\phi n(n+1)\sin\theta\,\pi_n(\cos\theta)\,\frac{r_n(\rho)}{\rho^2}\hat{\mathbf{e}}_r + \sin\phi\tau_n(\cos\theta)\,\frac{D_n^{(j)}(\rho)\,r_n(\rho)}{\rho}\hat{\mathbf{e}}_\theta + \cos\phi\,\pi_n(\cos\theta)\,\frac{D_n^{(j)}(\rho)\,r_n(\rho)}{\rho}\hat{\mathbf{e}}_\phi, \tag{2.3}$$

$$\mathbf{N}_{e1n}^{(j)} = \cos\phi n(n+1)\sin\theta\,\pi_n(\cos\theta)\,\frac{r_n(\rho)}{\rho^2}\hat{\mathbf{e}}_r + \cos\phi\tau_n(\cos\theta)\,\frac{D_n^{(j)}(\rho)\,r_n(\rho)}{\rho}\hat{\mathbf{e}}_\theta - \sin\phi\,\pi_n(\cos\theta)\,\frac{D_n^{(j)}(\rho)\,r_n(\rho)}{\rho}\hat{\mathbf{e}}_\phi, \tag{2.4}$$

where r_n represents one of the Riccati–Bessel functions (ψ_n and ζ_n), which are related with the spherical Bessel and Hankel functions by the expressions:

$$j_n(\rho) = \psi_n(\rho)/\rho, \qquad h_n^{(1)}(\rho) = \zeta_n(\rho)/\rho. \tag{3}$$

We have also replaced the derivatives of the Riccati–Bessel functions by their logarithmic derivatives ($D_n^{(1)} = \psi_n'/\psi_n$ and $D_n^{(3)} = \zeta_n'/\zeta_n$) because the latter are numerically stable whereas the former are not [17]. To the best of our knowledge, this is the first time that vector spherical harmonics are expressed in this way. This representation greatly improves convergence during the near-field calculations. Now, the expansions of the fields in the lth region are given by [17]:

$$\mathbf{E}_l = \sum_{n=1}^{\infty} E_n\left[c_n^{(l)}\mathbf{M}_{o1n}^{(1)} - i\,d_n^{(l)}\mathbf{N}_{e1n}^{(1)} + i\,a_n^{(l)}\mathbf{N}_{e1n}^{(3)} - b_n^{(l)}\mathbf{M}_{o1n}^{(3)}\right], \tag{4.1}$$

$$\mathbf{H}_l = \frac{k_l}{\omega\mu}\sum_{n=1}^{\infty} E_n\left[d_n^{(l)}\mathbf{M}_{e1n}^{(1)} + i\,c_n^{(l)}\mathbf{N}_{o1n}^{(1)} - i\,b_n^{(l)}\mathbf{N}_{o1n}^{(3)} - a_n^{(l)}\mathbf{M}_{e1n}^{(3)}\right], \tag{4.2}$$

where ω is the angular frequency and μ the magnetic permeability.

Following Bohren and Huffman's treatment [12], we can determine the expansion coefficients ($a_n^{(l)}$, $b_n^{(l)}$, $c_n^{(l)}$ and $c_n^{(l)}$) by applying the boundary conditions at all the interfaces:

$$(\mathbf{E}_{l+1} - \mathbf{E}_l)\times\hat{\mathbf{e}}_r = 0, \quad (\mathbf{H}_{l+1} - \mathbf{H}_l)\times\hat{\mathbf{e}}_r = 0, \tag{5}$$

where $r = r_l$ and $l = 1, 2, \ldots, L$. The orthogonality condition, together with the expressions for vector harmonics [Eqs. (2.1)–(2.4)], the field expansions [Eqs. (4.1), (4.2)], and the boundary conditions [Eq. (5)] yield four (or, more appropriately, two different sets of) independent linear equations in the expansion coefficients [17]:

$$d_n^{(l+1)}m_l\psi_n'(m_{l+1}x_l) - a_n^{(l+1)}m_l\zeta_n'(m_{l+1}x_l) - d_n^{(l)}m_{l+1}\psi_n'(m_lx_l) + a_n^{(l)}m_{l+1}\zeta_n'(m_lx_l) = 0, \tag{6.1}$$

$$c_n^{(l+1)}m_l\psi_n(m_{l+1}x_l) - b_n^{(l+1)}m_l\zeta_n(m_{l+1}x_l) - c_n^{(l)}m_{l+1}\psi_n(m_lx_l) + b_n^{(l)}m_{l+1}\zeta_n(m_lx_l) = 0, \tag{6.2}$$

$$c_n^{(l+1)}\psi_n'(m_{l+1}x_l) - b_n^{(l+1)}\zeta_n'(m_{l+1}x_l) - c_n^{(l)}\psi_n'(m_lx_l) + b_n^{(l)}\zeta_n'(m_lx_l) = 0, \tag{6.3}$$

$$d_n^{(l+1)}\psi_n(m_{l+1}x_l) - a_n^{(l+1)}\zeta_n(m_{l+1}x_l) - d_n^{(l)}\psi_n(m_lx_l) + a_n^{(l)}\zeta_n(m_lx_l) = 0. \tag{6.4}$$

These equations can be solved to obtain the following expressions for the expansion coefficients:

$$a_n^{(l)} = \frac{D_n^{(1)}(m_lx_l)\,T_1(m_{l+1}x_l) + T_3(m_{l+1}x_l)\,m_l/m_{l+1}}{\zeta_n(m_lx_l)\,U(m_lx_l)}, \tag{7.1}$$

$$b_n^{(l)} = \frac{D_n^{(1)}(m_lx_l)\,T_2(m_{l+1}x_l)\,m_l/m_{l+1} + T_4(m_{l+1}x_l)}{\zeta_n(m_lx_l)\,U(m_lx_l)}, \tag{7.2}$$

$$c_n^{(l)} = \frac{D_n^{(3)}(m_lx_l)\,T_2(m_{l+1}x_l)\,m_l/m_{l+1} + T_4(m_{l+1}x_l)}{\psi_n(m_lx_l)\,U(m_lx_l)}, \tag{7.3}$$

$$d_n^{(l)} = \frac{D_n^{(3)}(m_lx_l)\,T_1(m_{l+1}x_l) + T_3(m_{l+1}x_l)\,m_l/m_{l+1}}{\psi_n(m_lx_l)\,U(m_lx_l)}, \tag{7.4}$$

where

$$U(z) = D_n^{(1)}(z) - D_n^{(3)}(z) \tag{8.1}$$

$$T_1(z) = a_n^{(l+1)}\zeta_n(z) - d_n^{(l+1)}\psi_n(z) \tag{8.2}$$

$$T_2(z) = b_n^{(l+1)}\zeta_n(z) - c_n^{(l+1)}\psi_n(z) \tag{8.3}$$

$$T_3(z) = d_n^{(l+1)}D_n^{(1)}(z)\,\psi_n(z) - a_n^{(l+1)}D_n^{(3)}(z)\,\zeta_n(z) \tag{8.4}$$

$$T_4(z) = c_n^{(l+1)}D_n^{(1)}(z)\,\psi_n(z) - b_n^{(l+1)}D_n^{(3)}(z)\,\zeta_n(z)\,. \tag{8.5}$$

The electric and magnetic fields are finite at the origin. Only $j_n(kr)$ gives a finite, non-singular behaviour at this point; this implies that it is the only possible radial dependence occurring in the spherical wave expansion of the fields in the inner layer [12]. This can be understood in a more physical way by considering that there are no outward waves entering in the inner layer and gives an additional condition for the expansion coefficients: $a_n^{(1)} = b_n^{(1)} = 0$. Moreover, total external fields in the region outside the sphere can be obtained by the superposition of the incident and scattered fields, $\mathbf{E} = \mathbf{E}_i + \mathbf{E}_s$; $\mathbf{H} = \mathbf{H}_i + \mathbf{H}_s$. They can be expanded as [12,17]:

$$\mathbf{E}_i = \sum_{n=1}^{\infty} E_n\left[\mathbf{M}_{o1n}^{(1)} - i\mathbf{N}_{e1n}^{(1)}\right], \tag{9.1}$$

$$\mathbf{H}_i = \frac{k_l}{\omega\mu}\sum_{n=1}^{\infty} E_n\left[\mathbf{M}_{e1n}^{(1)} + i\mathbf{N}_{o1n}^{(1)}\right], \tag{9.2}$$

$$\mathbf{E}_s = \sum_{n=1}^{\infty} E_n\left[i\,a_n\mathbf{N}_{e1n}^{(3)} - b_n\mathbf{M}_{o1n}^{(3)}\right], \tag{9.3}$$

$$\mathbf{H}_s = \frac{k_l}{\omega\mu}\sum_{n=1}^{\infty} E_n\left[-i\,b_n\mathbf{N}_{o1n}^{(3)} - a_n\mathbf{M}_{e1n}^{(3)}\right]. \tag{9.4}$$

By comparing Eqs. (4.1), (4.2) and (9.1)–(9.4), we can find additional conditions: $c_n^{(L+1)} = d_n^{(L+1)} = 1$ (inward EM waves outside the particle must be equal to the incident field), $a_n^{(L+1)} = a_n$ and $b_n^{(L+1)} = b_n$, where a_n and b_n are the scattering coefficients.

3. Computational algorithm

Schematic representation of the algorithm is shown in Fig. 1. The first step for the determination of EM fields around and inside a multilayered sphere is the calculation of scattering coefficients, discussed elsewhere [17,26]. Next, we have to determine

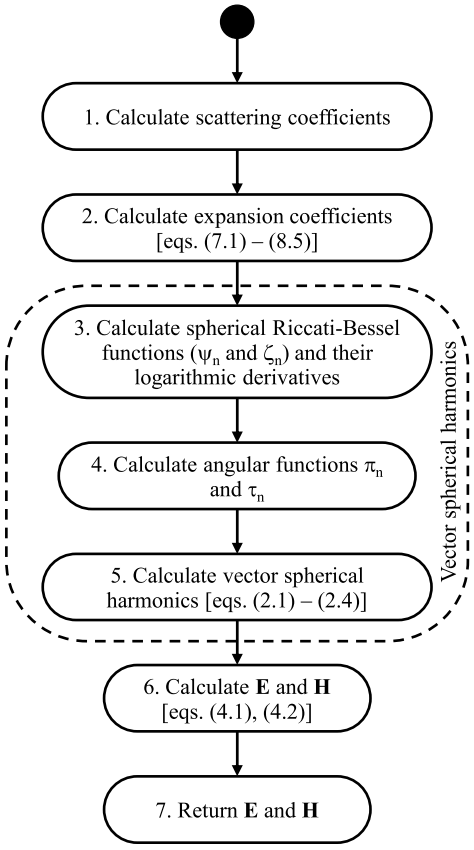

Fig. 1. Schematic representation of the algorithm for calculation of electric and magnetic fields.

the expansion coefficients by using expressions (7.1)–(8.5), starting with the outer layer and going iteratively down to the first one ($l = L, L-1, \ldots, 1$). Then, we must calculate the vector spherical harmonics [Eqs. (2.1)–(2.4)], which in turn requires the calculation of the angular functions π_n and τ_n, the Riccati–Bessel functions and their logarithmic derivatives. Angular functions do not pose any significant problem, and indeed, they have already been defined for the calculation of the far-field parameters [26]. Likewise, the calculation of the Riccati–Bessel functions and their logarithmic derivatives was already implemented and extensively tested in the previous version of *scattnlay* [26]. Finally, once the vector spherical harmonics have been calculated, we can apply expressions (4.1) and (4.2) for determining the electric and magnetic fields.

4. Computer program

The previous version of the program was written in ANSI C. This new version, however, has been ported to ISO C++11 due to the facilities offered by this language; in particular, objects and native complex math, and other data structures and algorithms provided in the standard library. To take advantage of this, the Mie calculation has been implemented in a C++ class (*MultiLayerMie*), but in order to keep compatibility with the previous version, we also defined wrapper functions to access all the functionalities, completely hiding the objects, at the choice of the user. The entire calculation core is defined in the files *nmie.h* and *nmie.cc*. The side effect of the porting was an increased performance of the calculations due to the program reorganization. As a result, the C++ version runs two times faster than the original C version for the same task.

In addition, there are some auxiliary files such as *farfield.cc* and *nearfield.cc* including all the necessary instructions to handle the data input/output to compile the software in two standalone programs (the executables are called *scattnlay* and *fieldnlay*) to perform far- and near-field calculations, respectively. Moreover, files *py_nmie.h*, *py_nmie.cc*, *setup.py*, *setup_cython.py*, *scattnlay.pyx* and *scattnlay.cpp* include wrapper functions to allow the compilation of the code as a Python extension. In this way, it is possible to take advantage of Python's plotting and data manipulation facilities coupled with the calculation core offered by our library. Finally, we have also included a *Makefile* to facilitate compilation, and several auxiliary files to compile the Python extension as either Debian (*.deb*) or Red Hat (*.rpm*) packages.

As for the calculation itself, there are three main functions for obtaining scattering coefficients and the far- and near-field parameters, as well as several auxiliary functions. The code is extensively commented, including a brief description of each function, its purpose, and the input/output parameters. In addition to the near-field calculations, the program can now deal properly with a layer of a perfect electrical conductor (PEC). Details of this new functionality have been discussed elsewhere [10].

5. Tests of the code

Several tests used to verify the accuracy of the far-field parameters were discussed in our previous paper [26]. All of these tests yielded the same results with the new code, ensuring that no precision was lost during the porting. In this work we are more concerned about the new code that calculates near electric and magnetic fields. Hence, we will skip the discussion over the far-field tests [26] and will focus exclusively on the new tests, related to the near-field calculations.

5.1. Silver nanoshell

The first test compares the results obtained from our code with those yielded by *BHFIELD* code, developed by Suzuki and Lee [24,25]. For this, we used both codes to calculate electric and magnetic fields for the example provided with their computer code: a silver nanoshell excited with wavelength 1064 nm. The exact conditions for the calculation were: $R_1 = 50$ nm, $R_2 = 60$ nm, $n_1 = 1.53413$, $n_2 = 0.565838 + i7.23262$ and $n_m = 1.3205$. The absolute enhancement of the electric field ($|\mathbf{E}|/|\mathbf{E}_0|$) is depicted in Fig. 2, as given by *BHFIELD* (Fig. 2(a)) and *scattnlay* 2.0 (Fig. 2(b)). The results yielded by both codes are virtually identical up to four significant digits. However, we consider that our code is a better choice even for the core-shell case. This advantage should arise for more complicated cases where our code is expected to have better accuracy because it avoids ill-behaved Bessel functions, which present well known convergence problems [17,27].

5.2. Power-flow lines in a silver nanoparticle

Bashevoy et al. [22] have reported the appearance of whirlpool-like nanoscale optical vortices around a silver nanoparticle for frequencies close to the localized surface plasmon resonance. Power-flow lines are defined as the lines to which the time-averaged Poynting vector $\mathbf{P} = 1/2\mathrm{Re}[\mathbf{E} \times \mathbf{H}^*]$ is tangential [22]. Electric and magnetic fields were calculated for a spherical silver nanoparticle using *scattnlay* and then a Python script was used to determine the streamlines $\mathbf{A}(t) = (x(t), y(t), z(t))$ of the time-averaged Poynting vector field, computed by integrating the differential equation: $d\mathbf{A}/dt = \mathbf{P}(\mathbf{A})$, where t is length of the path [22,28]. Results of the calculation are depicted in Fig. 3. The radius of the nanoparticle was defined as $r = \lambda/20$ and the

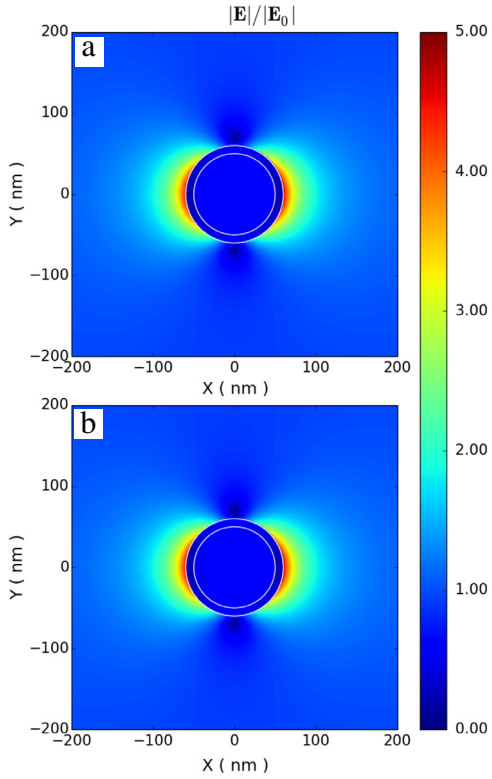

Fig. 2. Local field contour plot in the section plane for a silver nanoshell, as obtained from (a) *BHFIELD* and (b) *scattnlay*.

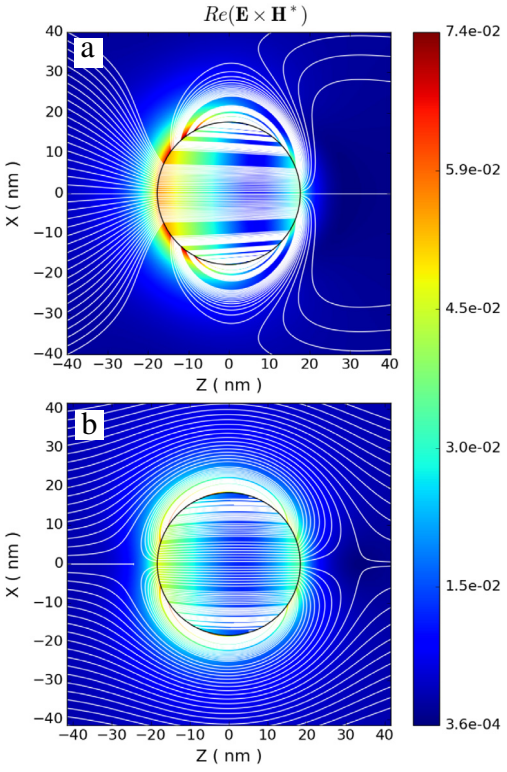

Fig. 3. Power-flow distribution around a spherical silver nanoparticle with radius of ∼20 nm ($\lambda/r = 20$) in the plane defined by the directions of propagation (from left to right) and polarization of the incident light. (a) $\lambda = 354$ nm and (b) $\lambda = 367$ nm. The colors indicate the absolute value of the Poynting vector and the white lines show the direction of power-flow.

calculations were performed for $\lambda = 354$ nm (Fig. 3(a), $\varepsilon = -2.0 + i0.28$) and $\lambda = 367$ nm (Fig. 3(b), $\varepsilon = -2.71 + i0.25$). Our results closely match those reported by Bashevoy et al. [22]; in particular, whirlpool-like vortices that appear in our local-field contours are nearly identical to those observed by them (their Figs. 2(c) and 2(d)). This match upholds the high accuracy of our algorithm and its implementation.

5.3. Power-flow lines in a dielectric coating

Finally, we determined the power-flow lines for a dielectric multilayered structure (32 layers) recently reported by us [10], where the near-field distribution was calculated using full-wave commercial 3D electromagnetic simulation software CST MWS [29]. This multilayer structure serves as an invisibility cloak and its refractive index was optimized to minimize scattering by the enclosed PEC sphere. In that work, we predicted the multilayer to reduce scattering by exhibiting a waveguide-like effect; i.e., by conducing the power-flow lines around the PEC sphere. Power-flow lines are plotted in Fig. 4 for the bare PEC sphere (Fig. 4(a)) and the multilayer structure (Fig. 4(b)). Calculations were performed for wavelength 3.75 cm and a PEC sphere with radius 2.81 cm (75% of wavelength); the multilayer is composed of 32 layers of the same thickness, having the refractive indices reported in Fig. 7 of our previous work [10]. The total thickness of the multilayer is 0.8 cm. The power-flow distribution plots show that EM waves are much less affected by the structure when the coating is present, reinforcing the results obtained in the far-field calculation.

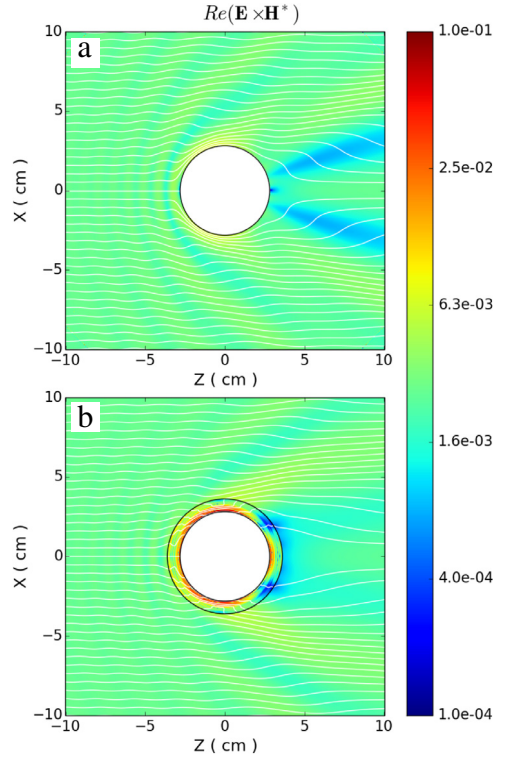

Fig. 4. Power-flow distribution around (a) a PEC sphere and (b) the same PEC sphere covered with an all-dielectric multilayer coating optimized to reduce scattering (RCS drop is 51.9%). The colors indicate the absolute value of the Poynting vector and the white lines show the direction of power-flow.

6. Conclusions

There are many Mie-type models and algorithms for solving the problem of EM scattering by core-shell and multilayered spheres in the far-field but the same is not true for the near-field. In this paper,

we report on the algorithm and corresponding implementation that we have developed for calculating near-fields (electric and magnetic) for a radially inhomogeneous sphere. The algorithm is stable and accurate for a large range of size parameters and material constants. Most of the stability gains arise from the use of the Riccati–Bessel functions and their logarithmic derivatives that, unlike Bessel functions, are stable and well behaved. Agreement between the results obtained with our algorithm and those reported in the literature or yielded by similar programs is very good. The proposed algorithm (implemented in *scattnlay* version 2.0) is fast, accurate, and capable of calculating the electric and magnetic fields inside and around a multilayered sphere. The new and the existing functionalities are all available in *scattnlay* 2.0, which can simulate all the relevant quantities to study the EM scattering by multilayer structures in the far- and near-fields. The algorithm and the resulting code will be very useful for a wide scientific community interested in the problem of EM scattering by a stratified sphere.

Acknowledgements

O.P.R. is grateful to Moncloa Campus of International Excellence (Spain) for the PICATA postdoctoral fellowship and Consejo Nacional de Ciencia y Tecnología (Mexico) for financing a short stay at Universidad Autónoma de Puebla, Mexico. This work was partially funded by the Spanish MINECO project Radiafus4 (ENE2015-70300-C3-3-R) and EUROfusion Consortium (AWP15-ENR-01/CEA-02). The authors thank the anonymous reviewers for their valuable comments.

References

[1] R.D. Averitt, D. Sarkar, N.J. Halas, Phys. Rev. Lett. 78 (1997) 4217. http://dx.doi.org/10.1103/PhysRevLett.78.4217.
[2] Y. Hu, R.C. Fleming, R.A. Drezek, Opt. Express 16 (2008) 19579–19591. http://dx.doi.org/10.1364/OE.16.019579.
[3] O. Peña-Rodríguez, U. Pal, J. Phys. Chem. C. 114 (2010) 4414–4417. http://dx.doi.org/10.1021/jp1001034.
[4] O. Peña-Rodríguez, A. Rivera, M. Campoy-Quiles, U. Pal, Nanoscale 5 (2013) 209–216. http://dx.doi.org/10.1039/C2NR32281A.
[5] L.R. Hirsch, R.J. Stafford, J.A. Bankson, S.R. Sershen, B. Rivera, R.E. Price, J.D. Hazle, N.J. Halas, J.L. West, Proc. Natl. Acad. Sci. USA 100 (2003) 13549–13554. http://dx.doi.org/10.1073/pnas.2232479100.
[6] J.Z. Zhang, J. Phys. Chem. Lett. 1 (2010) 686–695. http://dx.doi.org/10.1021/jz900366c.
[7] L.R. Allain, T. Vo-Dinh, Anal. Chim. Acta 469 (2002) 149–154. http://dx.doi.org/10.1016/S0003-2670(01)01537-9.
[8] P. Chýlek, V. Ramaswamy, R.J. Cheng, J. Atmos. Sci. 41 (1984) 3076–3084. http://dx.doi.org/10.1175/1520-0469(1984)041\protect$\relax\$3076:EOGCOT\protect$\relax)$2.0.CO2.
[9] J.V. Martins, P. Artaxo, C. Liousse, J.S. Reid, P.V. Hobbs, Y.J. Kaufman, J. Geophys. Res. 103 (1998) 32041–32050. http://dx.doi.org/10.1029/98JD02593.
[10] K. Ladutenko, O. Peña-Rodríguez, I. Melchakova, I. Yagupov, P. Belov, J. Appl. Phys. 116 (2014) 184508. http://dx.doi.org/10.1063/1.4900529.
[11] A.L. Aden, M. Kerker, J. Appl. Phys. 22 (1951) 1242–1246. http://dx.doi.org/10.1063/1.1699834.
[12] C.F. Bohren, D.R. Huffman, Absorption and Scattering of Light by Small Particles, Wiley-Interscience, Weinheim, ISBN: 0-471-29340-7, 1998.
[13] J.R. Wait, Appl. Sci. Res. B. 10 (1962) 441–450. http://dx.doi.org/10.1007/BF02923455.
[14] R. Bhandari, Appl. Opt. 24 (1985) 1960–1967. http://dx.doi.org/10.1364/AO.24.001960.
[15] Z.S. Wu, Y.P. Wang, Radio Sci. 26 (1991) 1393–1401.
[16] B.R. Johnson, Appl. Opt. 35 (1996) 3286–3296. http://dx.doi.org/10.1364/AO.35.003286.
[17] W. Yang, Appl. Opt. 42 (2003) 1710–1720. http://dx.doi.org/10.1364/AO.42.001710.
[18] D.W. Mackowski, M.I. Mishchenko, J. Quant. Spectrosc. Radiat. Transfer 112 (2011) 2182–2192. http://dx.doi.org/10.1016/j.jqsrt.2011.02.019.
[19] Z.S. Wu, L.X. Guo, K.F. Ren, G. Gouesbet, G. Gréhan, Appl. Opt. 36 (1997) 5188–5198. http://dx.doi.org/10.1364/AO.36.005188.
[20] L. Kai, P. Massoli, Appl. Opt. 33 (1994) 501–511. http://dx.doi.org/10.1364/AO.33.000501.
[21] S.J. Oldenburg, S.L. Westcott, R.D. Averitt, N.J. Halas, J. Chem. Phys. 111 (1999) 4729–4735. http://dx.doi.org/10.1063/1.479235.
[22] M.V. Bashevoy, V.A. Fedotov, N.I. Zheludev, Opt. Express 13 (2005) 8372–8379. http://dx.doi.org/10.1364/OPEX.13.008372.
[23] U. Zywietz, A.B. Evlyukhin, C. Reinhardt, B.N. Chichkov, Nature Commun. 5 (2014) 3402. http://dx.doi.org/10.1038/ncomms4402.
[24] H. Suzuki, I.-Y.S. Lee, Int. J. Phys. Sci. 3 (2008) 38–41.
[25] H. Suzuki, I.-Y. Sandy Lee, J. Quant. Spectrosc. Radiat. Transfer 126 (2013) 56–60. http://dx.doi.org/10.1016/j.jqsrt.2012.09.006.
[26] O. Peña, U. Pal, Comput. Phys. Comm. 180 (2009) 2348–2354. http://dx.doi.org/10.1016/j.cpc.2009.07.010.
[27] H. Du, Appl. Opt. 43 (2004) 1951–1956. http://dx.doi.org/10.1364/AO.43.001951.
[28] M. Dorobantu, Efficient Streamline Computations on Unstructured Grids, Department of Numerical Analysis and Computing Science, Royal Institute for Technology, Stockholm, 1997, http://citeseerx.ist.psu.edu/viewdoc/summary?doi=10.1.1.56.940.
[29] CST - Computer Simulation Technology, 2016. https://www.cst.com/ (accessed November 16, 2016).